A Section 508–conformant HTML version of this article
is available at https://doi.org/10.1289/EHP15010.

Projections of Heat-Related Mortality in Chinese Cities: The Roles of Climate Change, Urbanization, Socioeconomic Adaptation, and Landscape-Level Strategies

Xue Liu,[1] Ming Hao,[1] Yuyu Zhou,[2,3] Yue Zhang,[1] Ziheng Xu,[1] Xiaojuan Liu,[1,4] Yukun Gao,[5] Rui Li,[1] Han Zhang,[6] Xia Li,[1] Xiaoping Liu,[7] and Yuanzhi Yao[1,8]

[1]School of Geographic Sciences, East China Normal University, Shanghai, China
[2]Department of Geography, The University of Hong Kong, Hong Kong SAR, China
[3]Institute for Climate and Carbon Neutrality, The University of Hong Kong, Hong Kong SAR, China
[4]School of the Environment, The University of Queensland, Brisbane, Queensland, Australia
[5]School of Computer Engineering, Suzhou Vocational University, Suzhou, China
[6]Shanghai Real-Estate Science Research Institute, Shanghai, China
[7]School of Geography and Planning, Sun Yat-Sen University, Guangzhou, China
[8]International Center for Climate and Global Change Research, School of Forestry and Wildlife Sciences, Auburn University, Auburn, Alabama, USA

BACKGROUND: Physiological heat strain induced by extreme temperatures in cities has led to significant heat-related deaths. Although socioeconomic adaptation is suggested to mitigate this issue, its effectiveness is limited. Conversely, there is a lack of comprehensive evaluation on the effectiveness of landscape-level strategies for mitigating heat-related deaths.

OBJECTIVES: We developed a comprehensive modeling framework to estimate the impacts of environmental stresses and mitigating strategies on heat-related deaths in China's cities from 2016 to 2055.

METHODS: The framework assesses future heat-related deaths through five experiments considering the influences of climate change, urbanization, socioeconomic adaptation, and landscape-level strategies. We used extrapolated region-specific exposure–response functions (ERF) and recent advancement of geo-statistics for public health to generate urban patch level ERF curves. We used these curves and temperature and population data to generate future heat-related deaths with a 1-km resolution and conducted 5,000 Monte Carlo simulations for uncertainty analysis.

RESULTS: Our analyses estimated that heat-related mortality will increase from 136.5 ± 16.5 deaths per million in 2016 to 175.7 ± 27.5 deaths per million in 2055 under SSP2-RCP4.5 (shared socioeconomic pathways–representative concentration pathways) scenario and from 140.0 ± 21.4 deaths per million to 230.2 ± 38.7 deaths per million under SSP5-RCP8.5 scenario, despite socioeconomic adaptation and landscape-level strategies. Socioeconomic adaptation (reducing deaths by 18.4–64.1 per million) and landscape-level strategies (reducing deaths by 45.6–51.3 per million) significantly mitigate heat-related deaths with varying effectiveness across different income levels. Specifically, in high-income cities with dense populations, landscape-level strategies are 2.2–4.3 times more effective than socioeconomic adaptation. Within these cities, implementing the same landscape-level strategies in the high-density urban centers led to an additional reduction up to 4.9–6.8 deaths/km^2 in comparison with surrounding areas.

DISCUSSION: Our framework helps to systematically understand the effectiveness of landscape-level strategies in reducing heat-related mortality. Future sustainable city management should prioritize landscape-level strategies along with socioeconomic adaptation to support healthy and comfortable communities. https://doi.org/10.1289/EHP15010

Introduction

Epidemiological and human health studies[1–3] show that heat extremes can induce significant magnitudes of mortality and morbidity in global cities. According to the collected case histories of 16 European countries,[4] more than 70,000 additional heat-related deaths occurred during the summer of 2003. Heat extremes and hot weather can cause physiological heat strain at the individual level, which is described as the rise in core temperature, dehydration, and cardiovascular strain in a human health study.[5] In addition, evidence[2,5,6] demonstrates that higher ambient temperatures resulting from global warming could further aggravate this physiological heat strain and increase the number of associated deaths. For instance, a study[7] on mortality in India shows that climate change from 1960 to 2009 corresponds to a 146% increase in the possibility of heat-related deaths of more than 100 people. The future-projection studies[8–10] indicate that climate change, indirectly driven by anthropogenic activities, is projected to elevate global temperatures by 2–4.9°C[10–13] by the end of the 21st century, which could significantly increase future heat-related deaths. For instance, by the end of the 21st century, the average temperature in China[10] is projected to increase by 1.5°C under representative concentration pathway (RCP) 4.5 and 3.8°C under the RCP8.5 scenario in comparison with the historical period. This warming is projected to amplify the health burden of heat stress, with the attributable fraction of heat-related excess mortality—defined as the ratio of heat-related deaths to total deaths—rising from 1.9% in the 2010s to 3.1% under the RCP4.5 scenario and to 5.5% under RCP8.5 scenario by the 2090s. Besides, more than 27,900 additional estimated heat-related deaths annually in urban areas of China[11] could be induced by the additional warming from 1.5°C to 2°C.

As a direct impact of anthropogenic activities at the local scale,[2,5] accelerated urbanization[14–16] results in a ubiquitous occurrence of hot spots of heat-related deaths in metropolitan areas. Urbanization promotes a notable increase in local temperature and further intensifies physiological heat strain,[14,16] also known as the urban heat island (UHI) effect,[17] primarily because of the high density of impervious surface area constructed with poor thermal properties. A case study[18] shows that UHI-induced warming is about 40%–70% as strong as that caused by climate change. Moreover, a large number of populations gathering in the

Address correspondence to Xia Li. Email: lixia@geo.ecnu.edu.cn. And, Xiaoping Liu. Email: liuxp3@mail.sysu.edu.cn

Supplemental Material is available online (https://doi.org/10.1289/EHP15010).

The authors declare they have nothing to disclose.

Received 19 March 2024; Revised 29 April 2025; Accepted 12 May 2025; Published 13 June 2025.

urbanized areas[19,20] can also exacerbate human exposure to heat extremes. A few human health studies[6,21] have attempted to incorporate UHI-induced warming into the projection of future heat-related deaths, revealing a significant contribution of this temperature rise to the increase in nonaccidental mortality rate. For instance, Iungman et al.[6] demonstrated that 4.33% of summer nonaccidental mortality could be attributed to the UHI effects for 93 European cities in 2015.

In response to above global and local temperature rises, socioeconomic adaptation, quantified through per capita gross domestic product (GDP) changes following established methodologies,[11,12] promotes individual's purchasing capacities for cooling facilities and health care,[10,13,21–24] thereby improving their ability to adapt effectively during periods of extremely hot events,[12] which will enhance the human ability to cope with physiological heat strain and reduce heat-related deaths. However, the most vulnerable groups[5] in cities cannot afford the financial and environmental cost of air conditioning, electric fans, and cold water ingestion. Even in a society with significant socioeconomic improvement,[11,12] projections indicate that heat-related deaths could increase under future climate change. These findings demonstrate that relying solely on socioeconomic adaptation maybe insufficient to address the potential physiological heat strain.

Therefore, in response to the rising global and local temperatures, it is crucial to integrate additional mitigation strategies to effectively confront heat-related challenges. Evidence indicates that landscape-level strategies, including increasing vegetation coverage,[25,26] enhancing surface albedo,[27,28] improving roof reflectivity,[29,30] and implementing green roofs,[27,28] can effectively lower ambient temperature. These strategies alter local surface energy balance through three aspects[25,27,28]: evapotranspiration, shading effects, and altering solar radiation reflectivity. For instance, a continental-scale human health analysis[6] reveals that increasing urban tree coverage to 30% can prevent roughly 40% of UHI-induced heat-related deaths. However, very few studies have incorporated these landscape-level strategies into future heat-related death projections, which limits practical evaluation of future death reduction potential and hampers the formulation of related policies in urban areas (Table 1).

To fill this significant knowledge gap, we developed a modeling framework to conduct an investigation of heat-related deaths in China's cities, with consideration of climate change, urbanization, socioeconomic adaptation, and landscape-level strategies (Table 2). An analysis of future heat-related deaths reveals the critical potential of landscape-level strategies that remain understudied in predictive modeling for reducing mortality, especially in the high-density urban settlements of megacities with high income levels.

Methods

We projected heat-related deaths in China's cities under different scenarios of urban expansion, GDP levels, and population developments [shared socioeconomic pathways (SSP)] and greenhouse gas emission (RCP) scenarios during the warm seasons (May–October) from 2016 to 2055. The choice of 2055 as the projection end point was motivated by our objectives to assess near-term climate change and urbanization impacts on heat-related mortality, providing actionable insights for imminent adaptation strategies. This time frame also corresponds with numerous studies focusing on the 2050s, ensuring consistency with the existing body of research.[21,31,32] A previous study[33] has identified four Tier-1 SSP-RCP integrated scenarios, SSP1-RCP2.6, SSP2-RCP4.5, SSP3-RCP7.0, and SSP5-RCP8.5, as crucial for climate science research. In addition, numerous future temperature-related mortality projection studies[34–37] have used SSP2-RCP4.5 and SSP5-

Table 1. Summary of previous studies on region, baseline period, and factors affecting heat-related mortality, and comparison with this study.

Authors	Region	Baseline period	Climate change	Urbanization	Socioeconomic adaptation	Landscape-level strategies	Resolution
Kephart et al.[87]	Latin America	2002–2015	Historical period	×	×	×	City level
Ballester et al.[46]	Europe	2022	Historical period	×	×	×	Regional level
Hajat et al.[22]	Middle East and North Africa	2001–2020	SSP1-2.6, SSP2-4.5 SSP3-7.0, SSP5-8.5	×	×	×	Country level
Yang et al.[10]	China	2010s	RCP4.5 and 8.5	×	×	×	Regional level
Zhu et al.[21]	China	2010	RCP4.5 and 8.5	√	×	×	1.25° × 0.942°
Wang et al.[11]	27 metropolises of China	1986–2005	1.5 and 2°C global warming	×	√	×	City level
Rodrigues et al.[24]	Lisbon, Portugal	1986–2005	RCP8.5	×	√	×	City level
Jenkins et al.[23]	UK	2011	1.5, 2, 3 and 4°C warming	×	√	×	12 km × 12 km
Rai et al.[12]	Bavaria, Germany	1990–2006	SSP1-2.6 SSP3-7.0	×	√	×	City level
Iungman et al.[6]	European cities	2015	Historical period	√	×	√	City level
This study	China	2008–2012	RCP4.5 and RCP8.5	√	√	√	1 km × 1 km

Note: The √ means that the corresponding research has considered this factor. The symbol × means corresponding research has not considered this factor. RCP, representative concentration pathways; SSP, shared socioeconomic pathways.

Table 2. A protocol designed by stepwise increasing the influencing factors on heat-related deaths, including climate change, urbanization, socioeconomic adaptation, and landscape-level strategies under the SSP2-RCP4.5 and SSP5-RCP8.5 scenarios.

Experiment	Climate data	Urbanization	Socioeconomic adaptation	Landscape-level strategies	Description
I	Historical daily temperature	/	/	/	• Historical heat-related deaths during the baseline period (2008–2012) • Only consider historical air temperature
II	Future daily temperature under RCP4.5 and RCP8.5	/	/	/	• Estimating future heat-related deaths during 2016–2055 under the influence of climate change • Considering climate change under RCP4.5 and RCP8.5 scenarios • Each scenario includes 21 climate models
III	Experiment II	Future urban land under SSP2 and SSP5	/	/	• Estimating heat-related deaths under climate change and urbanization • Considering urbanization under SSP2 and SSP5 scenarios • Two integrated scenarios: SSP2-RCP4.5 and SSP5-RCP8.5
IV	Experiment II	Experiment III	Change of per capita GDP	/	• Future heat-related deaths under the influences of climate change, urbanization, and socioeconomic adaptation • Socioeconomic adaptation refers to the change rates of per capita GDP under SSP2-RCP4.5 and SSP5-RCP8.5 scenarios
V	Experiment II	Experiment III	Experiment IV	Tree cover Cool pavement Green roof Cool roof	• Future heat-related deaths under the influences of climate change, urbanization, future adaptation, and landscape-level strategies • The influences of four landscape-level strategies on temperature reduction: tree cover > cool pavement > green roof > cool roof

Note: The symbol "/" indicates that the corresponding factor was not considered in that specific experiment. GDP, gross domestic product; RCP, representative concentration pathways, describing a series of trajectories of different greenhouse gas concentrations in the future; SSP, shared socioeconomic pathways, which provide a range of possible future socioeconomic development pathways for the analysis of different scenarios in climate models.

RCP8.5 scenarios. Consequently, this study selected these two scenarios to maintain consistency with prior research.

We initially considered future temperature as having two components: climate change and urbanization-induced warming (Figure 1). Future air temperature due to climate change for each future urban patch was obtained from simulated climate data (referring to future air temperature at urban patch level) (Table S1). We then used a three-phase model to predict urban-induced

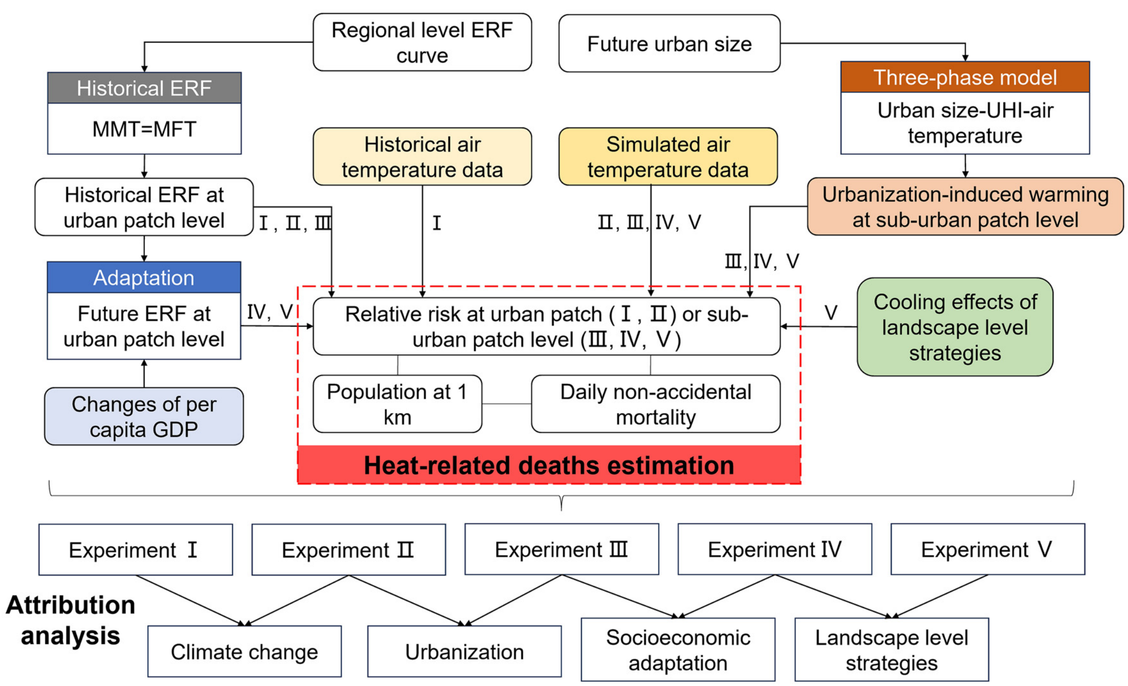

Figure 1. Flowchart of the proposed methodology in this study. This study designed five experiments, each with different input data. Subsequently, the differences between Experiment II and Experiment I, Experiment III and Experiment II, Experiment IV and Experiment III, as well as Experiment V and Experiment IV, were used as the attribute analyses for the impacts of climate change, urbanization, socioeconomic adaptation, and landscape-level strategies on heat-related mortality, respectively. Note: ERF, exposure–response functions; GDP, gross domestic products; MFT, most frequent temperature; MMT, minimum mortality temperature; UHI, urban heat island.

warming at the suburban patch level. Specifically, following the recent advancement of geo-statistics for public health,[11] we developed the spatially explicit exposure–response function (ERF) at the urban patch level. Finally, we integrated future temperature (urban patch level or suburban patch level resampled to 1 km), ERF (urban patch level), and future population (1 km) to provide a high-resolution (1 km) mapping of future heat-related deaths. We also conducted an attribution analysis to estimate the relative influence of the drivers on heat-related deaths. We conducted 5,000 Monte Carlo simulations to demonstrate the mean and standard deviation (SD) of heat-related deaths, illustrating the uncertainty in the results influenced by future climate models, urbanization-induced warming, and the cooling effects of landscape-level strategies. We used Python 3.13.1 (Python Software Foundation) to analyze five experiments and uncertainty results and ArcMap 10.5 (Esri) to create maps.

Data Sources

We collected data for this study from multiple sources (Table S2). We acquired the fifth generation European Center for Medium-Range Weather Forecasts atmospheric reanalysis of the global climate (ERA5) daily aggregates dataset to provide a globally complete and consistent dataset of daily mean temperature from 2005 to 2016 from Google Earth Engine Data Catalog (https://developers.google.com/earth-engine/datasets/catalog/ECMWF_ERA5_DAILY). In addition, future projected temperature data with a $0.25^\circ \times 0.25^\circ$ grid under RCP4.5 and RCP8.5 scenarios (Figure S1A) were obtained from the NASA Earth Exchange Global Daily Downscaled Climate Projections (NEX-GDDP) dataset under the Coupled Model Intercomparison Project Phase 5 (CMIP5),[18,38] which includes 21 General Circulation Model (GCM) runs provided by Google Earth Engine Data Catalog (https://developers.google.com/earth-engine/datasets/catalog/NASA_NEX-GDDP).

Then, we collected historical urban land data in 2015 from the Global Human Settlement Layer (GHSL) dataset,[39] daytime and nighttime land surface temperature (LST) data during the warm season of 2015 from Moderate Resolution Imaging Spectroradiometer (MODIS) MOD11A1 V6.1 (https://developers.google.com/earth-engine/datasets/catalog/MODIS_061_MOD11A1), air temperature of metrological stations during the warm season of 2015 from Global Historical Climatology Network-Daily (GHCND) version 3 dataset,[40] and impervious surface areas (ISA) with 30-m resolution from Global Annual Impervious Area (GAIA) dataset[41] in 2015 for China. Future urban land data for the future periods of 2020 (2016–2025), 2030 (2026–2035), 2040 (2046–2045), and 2050 (2046–2055), under the SSP2 and SSP5 scenarios (Figure S1B) from Chen et al.,[42] excluding areas smaller than $10\,km^2$. This dataset contains simulated urban patches (numbers between 1500 and 1700) in China across different years and scenarios, with an average area over $60\,km^2$. Future gridded population data under the same SSP scenarios, with a spatial resolution of 1 km for the same period, were extracted from a global population projections published by Li et al.[43] Future GDP data under the same SSP scenarios within the same period were obtained from the latest global gridded GDP projections published by Wang et al.[44] The above future population[43] and GDP[44] data were used to calculate future per capita GDP at the prefectural level (Figure S1C).

Baseline period (2008–2012) mortality rates and per capita GDP of 360 prefecture-level cities in China were collected from national or local Statistical Yearbooks (https://kns.cnki.net/kns8s/?classid=HHCPM1F8). We then sorted these values in ascending order. The quartile partitioning method was systematically applied as follows: *a*) Cities below the 25th percentile (≤15,921 yuan/person) formed the low-income group; *b*) the 25th–50th percentiles (15,921–23,575 yuan/person) composed the lower–middle-income group; *c*) the 50th–75th percentiles (23,575–38,136 yuan/person) constituted the upper–middle-income group; and *d*) cities above the 75th percentile (>38,136 yuan/person) formed the high-income tier. This quartile-based stratification ensured equal group sizes ($n = 90$ per tier) (Table S3). Three-dimensional building characteristics of 360 prefecture-level cities with building footprints and their corresponding building height in 2018 were collected from Baidu Map (https://lbsyun.baidu.com/). We used these building characteristics to identify the proportion of the base area of buildings <10 m in height in each prefecture-level city. These proportions were used to calculate the cooling effects of cool roofs and green roofs on the surrounding environment, because studies[29,45] have indicated that implementing cool roofs and green roofs on rooftops exceeding 10 m in height will not have an impact on outside ambient air temperature. The administrative boundaries of China (Map Approval Number: GS(2024)0650) were obtained from the National Geomatics Center of China (https://cloudcenter.tianditu.gov.cn/administrativeDivision/) as the base map.

Experiment Design

Based on previous studies,[6,10,11,21,46] we designed five experiments involving different input data to analyze heat-related deaths (Figure 1). We designed the sequence of factors for different experiments by synthesizing articles related to projections of temperature-related mortality (Table 2).

Experiment I used historical air temperature data and historical ERF curves at the urban patch level to estimate heat-related deaths during the period 2005–2015. The primary aim was to establish a reference baseline for subsequent comparisons.

Based on Experiment I, Experiment II employed simulated air temperature data to estimate heat-related deaths from 2016 to 2055. The mortality differential between Experiments II and I specifically isolated climate change impacts, assuming constant atmospheric forcing agents (aerosols, black carbon) and static population vulnerability parameters (demographic structure, health status).

In Experiment III, we extended Experiment II by incorporating urbanization-induced warming at the suburban patch level, derived from a three-phase model. The difference between Experiment III and Experiment II reflects the effects of future urban expansion–induced warming on heat-related mortality.

In Experiment IV, we integrated future temperature data, urbanization-induced warming, and the future ERF changes resulting from socioeconomic adaptations. The comparison of Experiment IV with Experiment III demonstrates the mitigating effects of future socioeconomic adaptations on heat-related mortality.

Experiment V introduced the cooling effects of landscape-level strategies based on the framework established in Experiment IV. The difference between Experiment V and Experiment IV estimates the potential effects of landscape-level strategies in reducing heat-related mortality.

Historical and Future Temperature Data

We used the ERA5 dataset during the historical period as the temperature data of Experiment I in Table 2. We obtained historical temperature data at urban patch level then resampled the data to a 1-km resolution. For future climate projections, we used the NEX-GDDP dataset during period 2016–2055 to provide future daily mean temperature data. Considering the deviations between the observed data (ERA5) and projected data (NEX-GDDP), we applied a bias-correction method[47] to correct systematic bias between the two datasets using the overlapping period of 2006–

2016. Then, we calculated the daily mean temperature of each future climate grid by averaging the daily minimum and maximum temperatures[10,48] of all 21 GCMs under the RCP4.5 and RCP8.5 scenarios, which represents medium and high greenhouse gas emissions, respectively, being two commonly chosen scenarios in previous studies.[34,49] Finally, we overlaid the future urban patches with the daily average temperatures to obtain the daily average temperature for each urban patch during the warm season (May–October) of each year from 2016 to 2055. These results resampled to a 1-km resolution were used as the input climate data of Experiments II, III, IV, and V.

Urbanization-Induced Warming Estimation

We estimated urbanization-induced warming using a three-phase model (Figure 2).

Phase 1: Relationship between urban size and UHI. In Phase 1, we used a log-linear model to establish the relationship between whole urban size (GHSL) and UHI (MOD11A1) in 2015. First, to ensure the accuracy of the spatial resolution of urban land data, we excluded areas smaller than $10\,\mathrm{km}^2$ to ensure the accuracy of the spatial resolution of urban land, aligning with previous study.[50] Second, we calculated UHI from May to October 2015 as the temperature difference between urban and rural areas. We then used a log-linear model to build the relationship in 2015 because several studies[51–53] demonstrated the nonlinear relationship between UHI and urban size. To better understand this correlation, we used the natural breaks method to perform binning, creating 20 bins by averaging the urban sizes and UHI intensities in each bin, as suggested by previous studies[18,54] (Figure S2):

$$\Delta \mathrm{LST} = \mathrm{a} \times \log US + b, \tag{1}$$

where US refers to the urban size of the urban patch, a is the slope of the fitted linear regression, b is the intercept.

Phase 2: Relationship between LST and air temperature. In Phase 2, we established a relationship between LST and air temperature to project future air temperature elevation, because human health impact assessments require air temperature exposure compatible with existing epidemiological studies instead of LST.[18,55] This LST-to-AT (air temperature) conversion focuses on establishing exposure metrics consistent with health models, not disregarding other meteorological factors (e.g., humidity, wind speed, and solar radiation). We selected 206 weather stations located in China and calculated the daily mean air temperature from the GHCND version 3 dataset for May to October 2015. We then established a linear regression between daily mean air temperature and daily mean LST data (Figure S3):

$$AT = c \times LST + d, \tag{2}$$

where AT is the daily mean air temperature, LST is the daily mean LST, c is the slope of the fitted linear regression, d is the intercept.

Therefore, the projection of future air temperature elevation of each urban patch caused by urbanization can be calculated as the combination of Equation 1 and 2 as follows:

$$\Delta AT = c \times (a \times \log US_t + b) \tag{3}$$

where ΔAT is the air temperature elevation of an urban patch induced by UHI due to urbanization of future year t.

Phase 3: Allocation of future air temperature elevation. In Phase 3, we allocated the predicted air temperature elevation of each urban patch, calculated using Equation 3, among different zones within the urban patch (suburban patch level) (Figure S4). It is unlikely that the entire patch could experience the same temperature increase. Based on previous studies,[56,57] we assumed that a future increase in ISA would be positively associated with future air temperature elevation.

First, following the study of Li et al.,[58] we: *a*) extracted the ISA of 2015 with 30-m resolution in China from GAIA dataset[41]; *b*) aggregated the ISA data to 1 km; *c*) generated a kernel density map of 1 km ISA data using a kernel density estimation (KDE) approach with a search radius of 5 km; *d*) normalized the KDE results to 0–1 scale, subdividing the entire urban patches into five zones (suburban patch level) with intervals of 0.2, where 0.8–1 was the Zone 5, and 0–0.2 was the Zone 1, as suggested by previous studies.[59,60]

Second, we calculated the proportions of each future urban patch within the five different zones: *a*) the surrounding areas (buffer) around the future urban patches were defined as three times the size of urban patch areas based on previous studies[57,61];

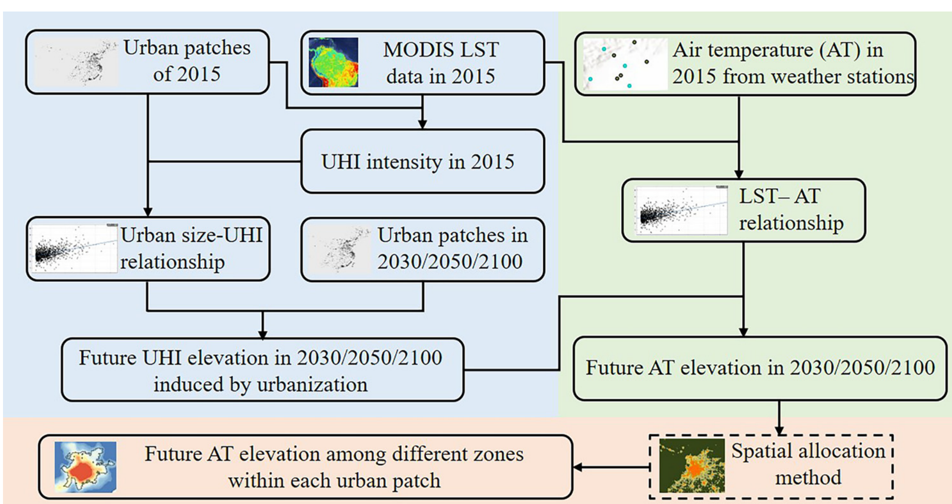

Figure 2. The three-phase model for predicting urbanization-induced warming and allocating temperature elevation within urban patches: an overview of Phases 1 (depicted in blue), 2 (depicted in green), and 3 (Depicted in orange). In Phase 1, this study built the relationship between urban size and UHI using log-linear regression. In Phase 2, this study established the relationship between LST and AT using linear regression. In Phase 3, the future AT elevation calculated from Phase 2 was allocated within different zones within each urban patch. The detailed allocation method is provided in Figure S2. Note: AT, air temperature; LST, land surface temperature; UHI, urban heat island.

these urban patches and their surrounding areas constituted the areas for proportion calculation; and *b*) we intersected these areas with the five different zones from the first part and computed the future urban patch proportion of each zone as the ratio of the area of urban land to the sum of urban land and surrounding areas.

Third, the allocation of future air temperature elevation to urban patches across different zones was performed based on their respective proportions as follows: *a*) we first calculated the area proportion of each zone relative to the whole urban patch; then, we multiplied each zone's area proportion by the future urban land proportion to derive the area-weighted coefficient for each zone; and *b*) we obtained the future air temperature elevation for the entire urban patch using Equation 3. *c*) Finally, we calculated the future temperature elevation for each zone based on the area-weighted coefficients and the temperature elevation for the urban patch.

After calculating the urbanization-induced warming, the future daily mean temperature considering the compound effects of climate change and urbanization on temperature (Experiment III, IV, and V in Table 2) was determined by summing the daily mean temperature from the NEX-GDDP dataset (urban patch level) and the air temperature elevation (suburban patch level) derived from the three-phase model, resampling the results to a 1-km spatial resolution.

We did not directly establish the relationship between urban size and UHI at the suburban patch level for the following reasons: the relatively poor fit of the binned linear relationship between the logarithm of urban size and UHI intensity across the five zones (Table S4) [this contrasts with the stronger relationship observed between whole urban patch size and UHI (Figure S2)]; and the slopes for Zones 1, 4, and 5 in Table S4 were found to be negative, suggesting that UHI intensity decreases as urban size increases, which is inconsistent with findings from previous studies.[51,57]

Historical ERF at the Urban Patch Level

A literature search was conducted to retrieve peer-reviewed studies published between 2010 and 2022 on the association between heat exposure and mortality in mainland China. Six relevant studies[10,21,62–65] providing regional ERF curves covering mainland of China were reviewed (Table S5). Considering the number of sample points used in establishing ERF curves across various studies, and the distribution balance of these sample points within each study's regions, we selected the ERF from Yang et al.,[10] which has the second largest number of sample points and the most balanced distribution (Table S5) across seven regions for this study. ERF represents the cumulative association between temperature and mortality, which is used to estimate the relative risks that urban patches will experience under future temperatures. First, we extracted the ERF curves in seven regions of mainland China from Yang et al.[10] using DataGrabber software (https://github.com/QY7/DataGrabber) to provide specific relative risk values for different temperatures across various regions. To ensure accuracy, two operators independently extracted data from the figures. If there was a discrepancy between their results, we averaged the two sets of results to reach a final value. These extracted associations were then applied as the regional ERFs in this study, indicating that urban patches in this study within the same region will have the same ERF.

However, significant spatial variability[62,66–68] in minimum mortality temperature (MMT) has been demonstrated. Assuming a fixed ERF curve for all urban patches within the same region would be unrealistic. To address this issue, we adopted the finding[69] of the most frequent temperature (MFT) of each urban patch as an alternative representation of MMT, which concluded that MFT closely resembles the local MMT for a given period.

$$MMT_{his} = MFT_{his}, \tag{4}$$

where MMT_{his} is the historical MMT, and MFT_{his} is the historical MFT.

To determine the MFT of each urban patch, we extracted the daily mean air temperature from the ERA5 dataset for baseline period. The MFT of each urban patch was then calculated as the mode of the daily mean temperatures within the 54th–92nd range of distribution[69] during the period 2008–2012 (ERA5). We subsequently adjusted the regional ERF curve derived from Yang et al.[10] to account for the spatial variability in MMT across urban patches (Figure S5).

Future ERF Considering Socioeconomic Adaptation

Under the same high temperature conditions, regions with higher socioeconomic levels[11,12] are better able to cope with associated higher heat risks. Therefore, future socioeconomic adaptation is considered a means of reducing the relative risk associated with high temperatures. In comparison with the baseline per capita GDP, the change in future per capita GDP, referring to the projected gross domestic product derived from Wang et al.,[44] can determine the change in the slope of ERF curve[12] (Figure S6). In this study, we employed the quadratic association between relative risk and per capita GDP under different heat intensities in China[11] to reflect the influence of future socioeconomic adaptation on ERF curves (Figure S7). By adjusting the historical ERF based on the future economic growth rate in comparison with the baseline period, we obtained the future ERF, which considers the future adaptation capacity improvements of each urban patch. It should be noted that using per capita GDP change as socioeconomic adaptation excludes direct effect of social improvement, including public cooling spaces, strengthening of primary health care, regulatory controls on occupational heat exposure, and early heat warning systems.

The Cooling Effects of Landscape-Level Strategies on Surrounding Temperature

We conducted a literature review (Table S6) of studies on the cooling effects of landscape-level strategies on surrounding temperature during the warm season across different climatic zones. Based on the results of Table S6, we presented the cooling effects of four landscape-level strategies, including tree cover, cool pavement, cool roofs, and green roofs, on surrounding air temperature (Table 3).

For instance, a study in Baltimore[70] demonstrated that a 10% increase in tree cover could reduce the monthly mean air temperature for summer months of June, July, and August by 0.19°C–0.4°C. Similarly, Pace et al.[71] suggested that a 10% increase in tree cover in Naples, Italy, generated a 0.2°C reduction in maximum hourly air temperature. A literature review[27] indicated that urban trees and hedges could lead to an average air temperature decrease ranging from 0°C to 3.5°C, with most reduction concentrated between 0.1°C and 1°C. After synthesizing the effects of tree cover on temperature reduction, we concluded that most studies conducted worldwide suggest that increasing urban tree cover by 10% can reduce air temperature by 0.1°C–0.4°C (Table 3). Using the same methodology, we also analyzed the impact of cool pavement, green roofs, and cool roofs on air temperature, with their value ranges detailed in Table 3.

When calculating the average reduction in heat-related mortality attributable to landscape-level strategies, we used the average cooling effect within the specified range for each strategy. For instance, increasing tree cover by 10% can reduce air temperature by 0.25°C in this study. These cooling effects were incorporated in Experiment V by reducing the temperature under the compound effects of climate change and urbanization on temperature elevation. In addition, given the variability in the cooling effects of different strategies, this study randomly selected values within the cooling range for each strategy during the uncertainty analysis (please refer to the section titled "Uncertainty Analysis").

Table 3. Basic description of landscape-level strategies and their cooling effects on surrounding air temperature.

Landscape-level strategies	Detailed description	Cooling effects	Spatial extent	Value set	Assumption	Sources
Tree cover	Increasing the tree coverage of the study area	Increasing by 10% can reduce the temperature by 0.1–0.4°C	The whole study area	10%	The increased tree cover is evenly distributed within the study area	Pace et al. (2022)[71] Sinha et al. (2021)[70] Wang et al. (2016)[30]
Cool pavement	Increasing the albedo of pavement	Increasing by 0.1 can reduce the temperature by 0.1–0.35°C	Pavement	0.3	The payment is evenly distributed in the study area, accounting for 35% of the area	Santamouris et al. (2017)[27] Santamouris & Fiorito (2021)[28]
Green roof	Increasing the tree coverage on the roof	Increasing green cover can reduce the temperature by 0.3–0.7°C	Roof	Whole roof	The roof is evenly distributed, accounting for 25% of the area.[79] This strategy has no impact on buildings above 10m[29]	Wang et al. (2016)[30] Santamouris (2014)[29] Santamouris et al. (2017)[27]
Cool roof	Increasing the albedo of roof	Increasing by 0.1 can reduce the temperature by 0.06–0.22°C	Roof	0.3	Same as green roof	Santamouris et al. (2017)[27] Santamouris & Fiorito (2021)[28] Aflaki et al. (2017)[79]

Note: Detailed information for the references used in this table can be found in Table S6.

Heat-Related Deaths Projection

In this study, we conducted one experiment (Experiment I) on heat-related deaths with a 1-km resolution during the baseline period and four experiments (Experiment II, III, IV, and V) on future heat-related deaths with a 1-km resolution from 2016 to 2055 under the SSP2-RCP4.5 and SSP5-RCP8.5 scenarios by integrating population data (1 km), daily nonaccidental mortality rates (urban patch level), and relative risk derived from ERFs associated with daily mean temperature (resampled to 1 km)[13] (Figure 1):

$$HD_{i,d,t} = \begin{cases} \dfrac{POP_{i,t} \times (RR_{i,d,t} - 1) \times NMR_{m,i,c}}{RR_{i,d,t}} & T_{i,d,t} > MMT \\ 0 & T_{i,d,t} \le MMT \end{cases} \quad (5)$$

and

$$HD_{c,t} = \sum\nolimits_{i=1}^{n} \sum\nolimits_{d=1}^{184} HD_{i,d,t}, \quad (6)$$

where $HD_{i,d,t}$ is the heat-related deaths of pixel i at day d of year t; $POP_{i,t}$ is the population of pixel i at year t; $RR_{i,d,t}$ is the relative risk of pixel i at day d of year t, which is derived from historical/future ERF associated with daily mean temperature (more details can be found in the section titled "Historical ERF at the Urban Patch Level"); $NMR_{m,i,c}$ is the daily nonaccidental mortality rate in the baseline period of pixel i in city c, which is calculated by multiplying the annual nonaccidental mortality rate in city c by the monthly mortality proportions (May–October) then divided by days in month m[13]; the annual nonaccidental mortality rate in the baseline period of city c is calculated by multiplying the prefectural mortality rates from the Statistical Yearbooks by China's proportion of nonaccidental deaths obtained from the Global Burden of Disease study[21]; $T_{i,d,t}$ is the daily mean temperature of pixel i at day d of year t; MMT is the minimum mortality temperature derived from the lowest point of historical/future ERF curves, referring to the temperature having the lowest relative risk; and $HD_{c,t}$ is the heat-related deaths of city c at the year t from May to October (total 184 d), which is the sum of the heat-related deaths of all n pixels within city c from May to October at year t. After estimating the annual heat-related mortality for the years 2016–2055, we employed linear regression to fit the relationship between the year and mortality rates. We assessed the statistical significance of the linear trend based on a p-value (from the t-test) <0.01.

Uncertainty Analysis

We evaluated uncertainty originating from three major sources in estimating future heat-related deaths, including future climate change models, urbanization effects, and parameters for landscape-level strategies.

Previous studies[6,21] have suggested that climate change and urbanization have a compounding effect on heat-related deaths. To evaluate the uncertainties associated with future climate change and urbanization effect, we conducted a Monte Carlo simulation consisting of 5,000 repetitions of experiments per year over the period from 2016 to 2055. For climate change, daily temperature data was randomly selected from one of the 21 GCMs, and this process was repeated 5,000 times. For urbanization, we quantified uncertainty induced by the three-phase model of evaluating urbanization-induced warming by 5,000 repetitions. Because urbanization-induced warming uncertainty mainly originated from the fitting models, the ranges of three coefficients (coefficients of a, b, c in Equation 3) can be found in Figures S2 and S3. The results of uncertainty of climate change and urbanization can be found in Figure S8 (red shaded areas).

Furthermore, we identified the ranges of the landscape-level strategies on cooling effects in Table 3. Then, we conducted a Monte Carlo simulation to predict a set of 5,000 parameter pairs of landscape-level strategies from 2016 to 2055, keeping other drivers consistent with attribution analysis. The results of uncertainty of landscape-level strategies can be found in Figure S8 (green shaded areas).

Theoretically, uncertainties from climate change and urbanization and the cooling effects of landscape-level strategies are independent of each other; thus their joint uncertainty was calculated as the square root of the quadratic sum of the above two uncertainties[72] (Figure 3A). All analytical code and data processing scripts are publicly available in the GitHub repository at https://github.com/meipiao/EHP15010-code.

Results

Near Future Heat-Related Deaths

Our results indicate that the heat-related deaths are projected to show significant (linear regression, $p = 0.0001$) increasing trends

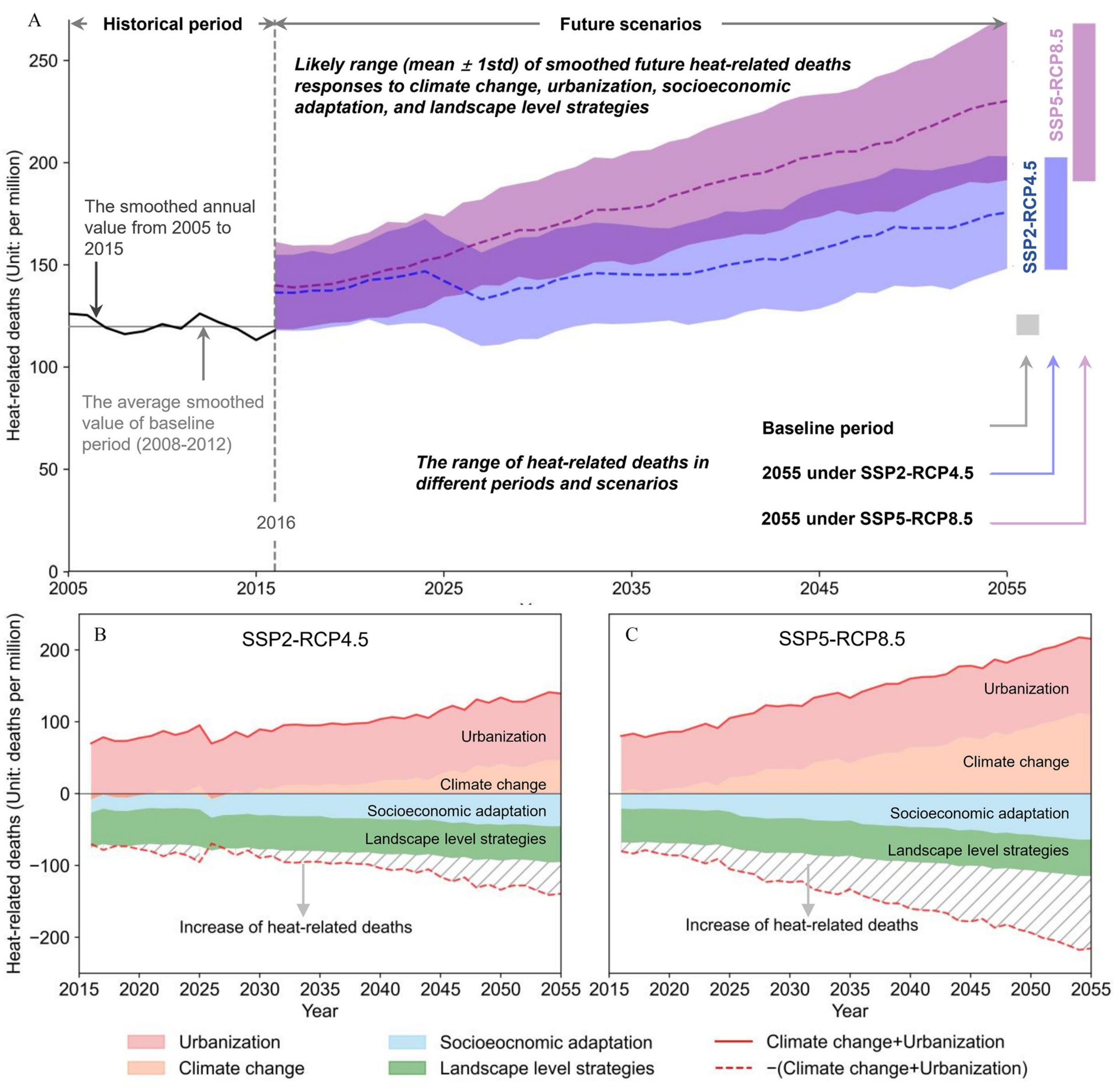

Figure 3. The near future heat-related deaths in the urbanized area of China. (A) the 3-y average smoothed heat-related deaths estimation (Experiment I) during the period 2005–2015 based on historical climate data, urban patch level ERF, and prefectural level mortality rates; and the 3-y average smoothed heat-related deaths estimation (Experiment V) during the period 2016–2055 based on future climate data, urbanization, socioeconomic adaption, and landscape-level strategies under the SSP2-RCP4.5 and SSP5-RCP8.5 scenarios with uncertainty ranges (mean ± 1 SD). The influences of climate change, urbanization, socioeconomic adaptation, and optimal landscape-level strategies on heat-related deaths under the SSP2-RCP4.5 scenario (B) and SSP5-RCP8.5 scenario (C). Numeric data can be found in Excel Tables S1–S3. Note that the tipping point refers to the time at which the future heat-related deaths exceed those during the baseline period for the first time. Note: RCP, representative concentration pathways; SD, standard deviation; SSP, shared socioeconomic pathways.

from 2016 to 2055 under two integrated scenarios (Figure 3A). The projected annual heat-related deaths would increase from 136.5 ± 16.5 per million in 2016 to 175.7 ± 27.5 per million in 2055, at an average growth rate of 0.98 per million/y under the SSP2-RCP4.5 scenario (Figure 3A; Excel Table S1). Under the SSP5-RCP8.5 scenario, the projected heat-related deaths would show an increasing trend, with the total magnitude increases from 140.0 ± 21.4 per million in 2016 to 230.2 ± 38.7 per million in 2055, at an average growth rate of 2.26 per million/y.

Under the SSP2-RCP4.5 scenario, urbanization explains most of the estimated increase in heat-related deaths during the period 2016–2025, with an annual average magnitude of 80.3 per million (Figure 3B; Excel Table S2). Although the contribution of climate change to the estimated increase of heat-related deaths is minimal (annual average of 0.1 per million). During the years 2046–2055, urbanization would be responsible for an estimated annual average of 91.1 per million heat-related death increases, followed by climate change (39.1 per million). In addition, during the period 2016–2025, the estimated contribution of landscape-level strategies and socioeconomic adaptation on heat-related deaths would be an annual average of −49.7 and −19.9 per million. During the years 2046–2055, socioeconomic adaptation would account for an estimated annual average of 43.0 per million in heat-related death reduction, and the contribution of landscape-level strategies would account for an estimated annual average of 49.1 per million in death reduction.

Under the SSP5-RCP8.5 scenario, urbanization again plays the most important role in explaining the estimated increase in heat-related deaths in 2016–2025 (annual average of 78.8 per million), followed by climate change (9.4 per million) (Figure 3C; Excel Table S3). During years 2046–2055, the impact of urbanization on projected heat-related deaths increases substantially, with an annual average of 102.3 per million, followed by climate change (95.3 per million). Furthermore, socioeconomic adaptation would reduce annual heat-related deaths by 58.5 per million during 2046–2055, compared to a reduction of 22.2 per million in 2016–2025. In addition, landscape-level strategies would reduce the annual average of projected heat-related deaths by 47.4–49.6 per million in the same time period.

Variations among Income Levels

We investigated the contribution of the four driving forces on heat-related deaths among four income levels (high-income level, upper-middle income level, lower-middle income level, and low-income level) (Figure 4; Excel Table S4). Climate change, a global-scale phenomenon, does not have a large difference among income levels, even though the changes in climate conditions show large spatial variations (Figure 4A,E; Figure S9). In high-income cities, where the majority are megacities with dense populations, climate change would contribute to an estimated annual average of 27–69 per million heat-related deaths during 2046–2055 under two scenarios. In addition, climate change contributes to an estimated annual average of 79–126 per million heat-related deaths in the lower-middle income level.

Moreover, the influence of urbanization on the increase in heat-related deaths shows an upward trajectory in tandem with the rise in income levels (Figure 4B,F; Figure S9). In high-income cities, urbanization would contribute to an estimated annual average of 71–82 per million heat-related deaths during the period 2046–2055 under two integrated scenarios, whereas in low-income cities, usually small cities with sparse populations, it leads to an estimated annual average of 49–57 per million heat-related deaths.

The influence of socioeconomic adaptation on heat-related deaths represents an upward trend from high-income level to low-income level (Figure 4C,G; Figure S9). In high-income

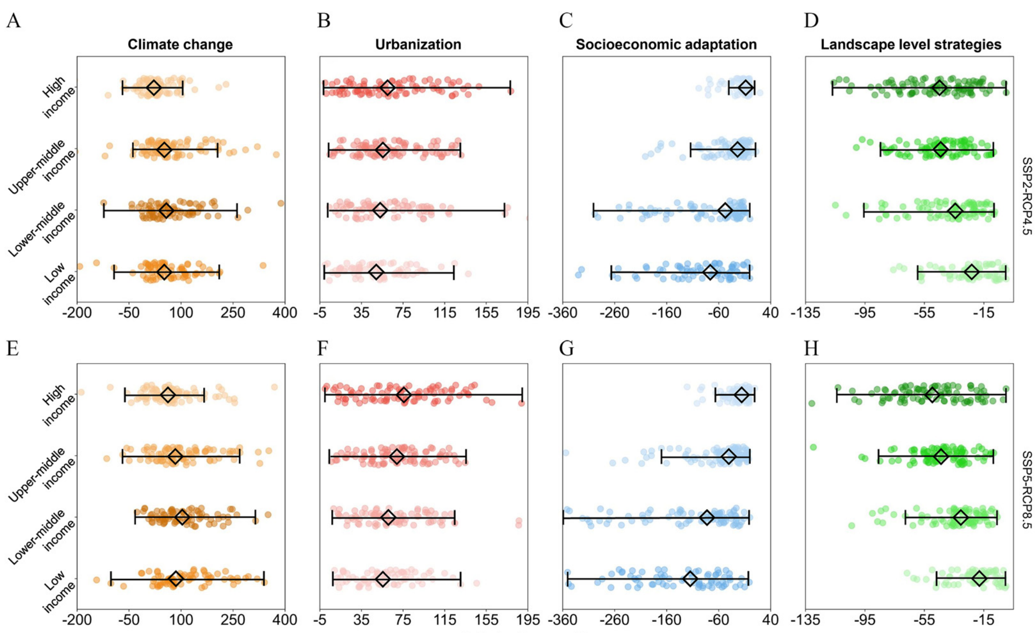

Figure 4. Attribution analysis of heat-related deaths among four income levels, 2046–2055. A box plot illustrates the effects of climate change, urbanization, socioeconomic adaptation, and landscape-level strategies on heat-related deaths in different cities. We collected and ranked the per capita GDP of 360 cities. However, due to the varying sizes of the urban patches (area $\geq 10\,km^2$), not all cities were included in the study. A total of 332 cities were selected for analysis. Numeric data can be found in Excel Table S4. Each solid colored dot represents a different city's location. The center of the diamond denotes the median of the box plot, while the lines extending from the diamond indicate the maximum and minimum normal values (upper and lower whiskers). Data points beyond the whiskers are identified as outliers. (A) The impacts of climate change, (B) urbanization, (C) socioeconomic adaptation, (D) landscape-level strategies on heat-related deaths under the SSP2-RCP4.5 scenario, (E) climate change, (F) urbanization, (G) socioeconomic adaptation, and (H) landscape-level strategies on heat-related deaths under the SSP5-RCP8.5 scenario 2046–2055.

cities, future socioeconomic adaptation is projected to reduce an annual average of 14–23 deaths per million heat-related deaths, which is substantially lower than that in the low-income cities with an estimated reduction of 102–141 per million heat-related deaths.

We find a substantial contribution of landscape-level strategies to the projected reduction of heat-related deaths, especially in high-income cities (Figure 4D,H; Figure S9), where landscape-level strategies are capable of reducing the estimated annual average of heat-related deaths by 48–51 per million under the SSP2-RCP4.5 and SSP5-RCP8.5 scenarios during the years 2046–2055. In contrast, in low-income cities, landscape-level strategies can potentially only achieve an estimated reduction of an annual average of 22–26 deaths per million during the same period.

Differences along Urban-Rural Gradients

Our finding indicates that the effect of the mixed effects (combined climate variability, urbanization, and socioeconomic adaptation) on the estimated increase in heat-related deaths exhibits a gradual increase from the rural areas (low-density population) to the urban centers (high-density population) (Figure 5; Figures S10 and S11), and the landscape-level strategies on estimated heat-related death reduction show the same trend.

Taking the SSP2-RCP4.5 scenario during the years 2046–2055 as an example, the potential effect of landscape-level strategies on projected heat-related death reduction would increase from an annual average of 0.01 death/km^2 in the rural areas to 0.94 death 0.94 death/km^2 in the urban areas in the Beijing–Tianjin–Hebei region (Figures 5B and 6B). This trend becomes more pronounced in the Yangtze River Delta (Figure 5F) and Pearl River Delta (Figure 5J), where the projected magnitude of heat-related death reduction increases to 4.9 $\text{deaths}/\text{km}^2$, and 6.8 $\text{deaths}/\text{km}^2$ in the urban centers, respectively. Moreover, the influence of mixed effects on the projected increase in heat-related deaths would potentially increase from an annual average of -0.02 death/km^2 in rural areas to 2.4 $\text{deaths}/\text{km}^2$ in the urban centers in the Beijing–Tianjin–Hebei region, 12.7 $\text{deaths}/\text{km}^2$ in the Yangtze River Delta, and 11.6 $\text{deaths}/\text{km}^2$ in the Pearl River Delta (Figures 5 and 6A).

We also observed that the contribution of landscape-level strategies and mixed effects on estimated heat-related deaths changes over time. For instance, under the SSP5-RCP8.5 scenario during the years 2026–2035, landscape-level strategies can lead to an estimated reduction of 0.9 death/km^2 in the urban centers of the Beijing–Tianjin–Hebei region (Figure 5C). During 2046–2055, it is estimated that the magnitude would increase to 1.1 death/km^2 (Figure 5D). Moreover, mixed effects can lead to a potential increase of 1.7 $\text{deaths}/\text{km}^2$ in the urban centers of Yangtze River Delta during 2026–2035 (Figure 5G). During the period 2046–2055, this magnitude would potentially increase to 2.5 $\text{deaths}/\text{km}^2$ (Figure 5H).

Discussion

To the best of our knowledge, this study represents a comprehensive investigation to date of the factors, including climate change, urbanization, socioeconomic adaptation, and landscape-level strategies, influencing heat-related deaths (Table 2). The performance of our modeling framework, specifically the reliability of

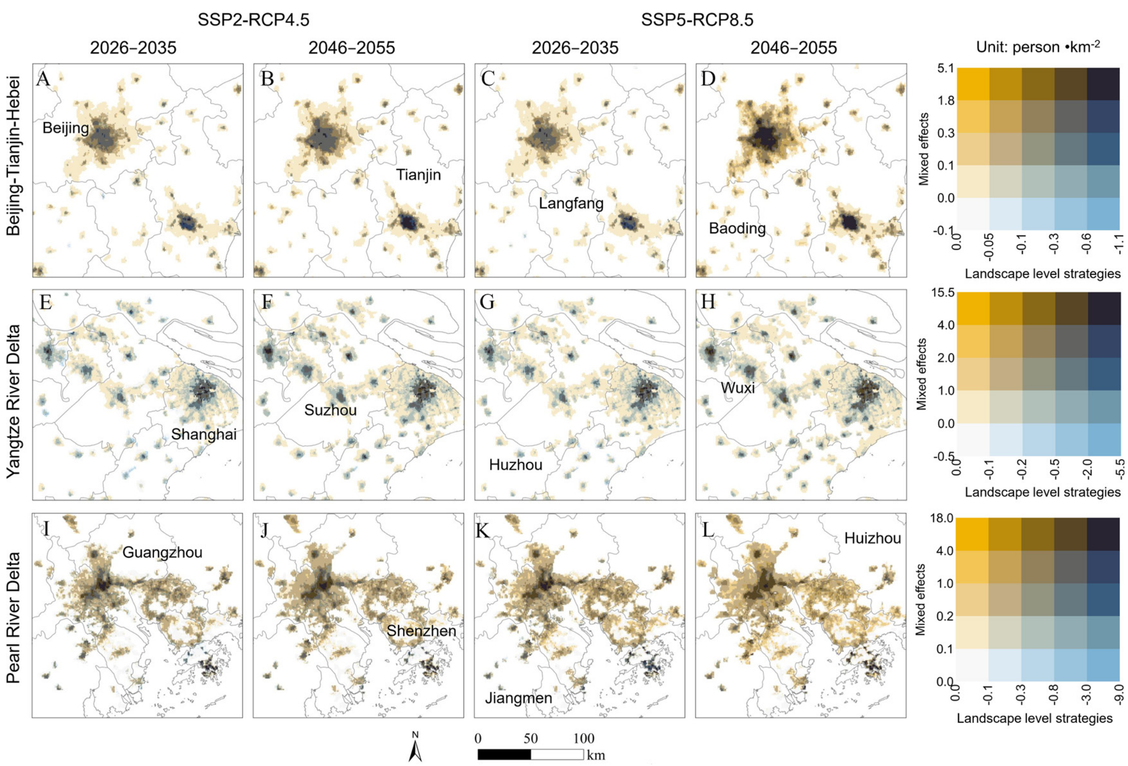

Figure 5. The spatial distribution of influence of mixed effects and landscape-level strategies on annual mean heat-related deaths at a resolution of 1 km × 1 km in the Beijing–Tianjin–Hebei region (A–D), the Yangtze River Delta (E–H), and the Pearl River Delta (I–L). Note that the mixed effects refer to the combined effects of climate change, urbanization, and socioeconomic adaptation on heat-related deaths. The mixed effects and landscape-level strategies were spatially visualized using a 2-dimensional legend to intuitively demonstrate the mitigating impact of landscape-level strategies on heat-related deaths. Numeric data can be found in Excel Table S5. The units represent the impacts of mix effects and landscape-level strategies on heat-related deaths. For instance, in the Yangtze River Delta, the maximum value of mixed effects is 15.5, which represents an increase of up to 10.5 heat-related deaths per square kilometer due to mixed effects. Conversely, the minimum value for landscape-level strategies in the same region is -5.5, suggesting a maximum decrease of 5.5 heat-related deaths per square kilometer due to landscape-level strategies.

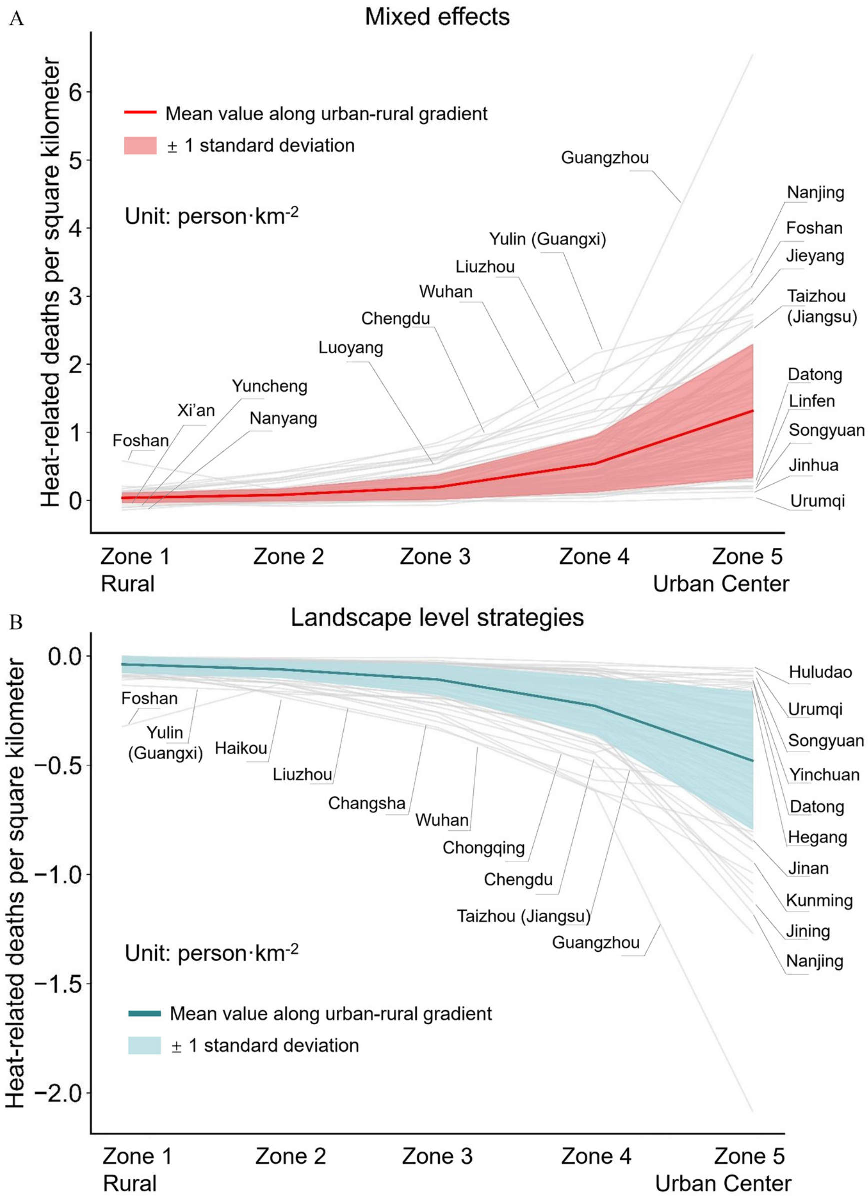

Figure 6. The influences of mixed effects (A) and landscape-level strategies (B) on heat-related deaths along urban-rural gradient among different China's cities during the period 2046–2055 under the SSP2-RCP4.5 scenario. To elucidate the spatial variations of mixed effects and landscape-level strategies on heat-related mortality across urban-rural gradients, Zone 5 obtained via the KDE method was regarded as the urban center of each urban patch and Zone 1 as rural. Summary data can be found in Excel Table S6. Note that the value on the *y*-axis represents the average number of heat-related deaths per square kilometer along the urban-rural gradient. Due to the KDE classification being based on normalized values ranging from 0 to 1, not all 332 cities have patches with all five levels. Therefore, this figure finally displays the 100 cities that contain all 5 levels of partitioning. Note: KDE, kernel density estimation.

the attribution analysis in estimating heat-related deaths, can be supported by previous studies.[6,18,21] We estimated that climate change (RCP4.5 and 8.5 scenarios) may contribute to an additional 39.1–95.3 per million heat-related deaths during the period 2046–2055 in comparison with the baseline period (2008–2012). This finding is consistent with a national level study[11] conducted in China, which reported a range of 71.6–97.8 per million for 1.5°C global warming under various SSPs. Similarly, a local human health study[73] conducted in Jiangsu Province reported a projected magnitude of 67 and 81 per million in the years 2041–2065 under the RCP4.5 and 8.5 scenarios, respectively, relative to the period of 2016–2040. Moreover, a recent study[74] analyzing temperature-related mortality across 854 European cities reveals that 13 countries in Europe experienced more than 140 heat-related deaths per million inhabitants annually during the period 1990–2019 attributable to climate change impacts. Furthermore, our results indicate that urbanization is the primary contributing factor to the increase in heat-related deaths, which is consistent with previous descriptive statements.[6,18,21]

Evidence[11] in China shows that socioeconomic adaptation can reduce heat-related deaths to 54.9–62.8 per million for 1.5°C global warming under various SSPs, which is slightly higher than our estimation (43.0–58.5 per million during the period 2046–2055). This difference can be attributed to the data source of future population and GDP, whereas we used the most updated gridded population and GDP data with higher resolution and improved prediction model in comparison with previous studies.[11,43,44] Certainly, the health benefits of socioeconomic development exhibit temporal heterogeneity, with diminishing marginal returns emerging at higher development levels.[75] Although China's rapid GDP growth historically coincided with substantial health improvements (e.g., health care accessibility and infrastructure), its transition toward high-income status could weaken this linkage, mirroring patterns in countries like Japan,[76] where macroeconomic trends and heat-related mortality became increasingly decoupled in recent decades. More important, our study suggests that 48%–63% of urbanization-induced deaths can be avoided when implementing optimal landscape-level strategies, where increasing tree coverage can reduce by 20%–26% of urbanization-induced deaths. Although no current study considers all the landscape-level strategies in large-scale estimations, our result referring to the effects of increasing tree coverage are somewhat lower than that in Iungman et al.[6] conducted in European cities (showing that roughly 40% of urbanization-induced deaths can be avoided). Two potential explanations can be posited for this discrepancy. First, the phenomenon of urbanization-induced warming may lead to elevated temperatures within urban centers, thereby contributing to increased mortality associated with urbanization in our study. Second, our target for enhancing tree cover is set at 10%, in stark contrast to the more ambitious goal of 40% established by Iungman et al.[6] It is notable that many urban areas with relatively low baseline tree cover (i.e., below 30%) are likely to experience a more pronounced increase in tree canopy coverage.

Implementing appropriate urban planning programs is critical for reducing heat-related deaths in cities. "Greenworks Philadelphia,"[77] a well-known urban planning program, established a goal of achieving 30% vegetation cover per neighborhood in 2009, which has been shown to significantly prevent premature deaths. Similarly, the "Consultancy Study on Building Design that Supports Sustainable Urban Living Space in Hong Kong"[78] clearly prescribed that 20%–30% of the building area should be designated for greenery, aiming to enhance environmental sustainability and mitigate heat-related impacts. In other regions of the world, analogous landscape-level strategies have been proposed for increasing vegetation cover, such as the "Kuala Lumpur Structure Plan"[79] 2020 in Malaysia, and the "Urban Greening Plans"[25] proposed by the European Commission. Our study highlights the importance of landscape-level strategies in the high-density urban settlements of megacities with high-income level. Besides tree coverage, other factors also influence the cooling effectiveness of urban greening, including tree canopy structure,[80] tree species,[81] and water use strategies.[82] A study[80] demonstrates that tree height, canopy cover above roads, canopy volume over roads, and leaf area index are positively correlated with road air temperature difference. In addition, research by Irmak et al.[81] reveals significant differences in urban temperature mitigation effects among different tree species. Moreover, adopting different water use strategies[82] can affect trees' transpiration and shading capacity, thereby altering their effects on ambient temperature.

During the baseline period, urban residents in high-income cities already had advanced public cooling infrastructure and had the financial capacity to acquire cooling equipment, such as air conditioning. Consequently, future economic improvements in high-income cities are expected to have ineffective effects in further reducing heat-related deaths. In contrast, a substantial enhancement in cooling capabilities is anticipated in low-income cities, which will likely result in a more pronounced decrease in heat-related deaths as economic conditions improve. Given that landscape-level strategies can induce similar cooling effects in both contexts, there exists a considerable potential to mitigate heat-related mortality and enhance public health outcomes in high-income cities as well. Implementing landscape-level strategies aims to create a healthy and comfortable environmental for all the groups.

It is evident that prioritizing the implementation of landscape-level strategies can significantly reduce heat-related deaths, especially in the high-density urban settlements (Figures 5 and 6); however, the estimated number will still rise irreversibly in comparison with the baseline period in both scenarios in this study. Therefore, cities could prioritize enhancing urban green infrastructure through targeted greening initiatives to achieve short-term mortality reduction. For instance, implementing ambitious tree canopy expansion goals[77] (e.g., 15%) in neighborhoods with limited existing vegetation could significantly improve heat mitigation outcomes. Besides, the increase of tree coverage should be coordinated following the local distribution of the population,[43,83,84] because this can effectively target areas with high population density and maximize the benefits of heat mitigation and environmental justice.[85,86] In addition, except the landscape-level strategies we mentioned in this study, other strategies,[5] including wetland restoration, urban ventilation pathways, and green traffic infrastructure, can be implemented in the future.

This study has several limitations. First, this study did not consider the impact of income disparities within urban patches on heat-related deaths. Future research should involve the heat risks faced by different income groups within cities, because this represents a significant issue in the study of urban environmental injustice. Furthermore, we did not account for the differential responses to heat risk across age and gender demographics. Subsequent work should aim to derive unique ERF curves for distinct age and gender groups. In addition, it is crucial to incorporate population simulation data that account for large-scale migrations driven by climate change to accurately estimate heat-related mortality. Last, although we defined a 6-month period (May–October) for evaluating heat-related deaths, it is possible that elevated temperatures occurring outside this time frame may lead to a minor underestimation of the associated mortality.

In this study, we provide a high-resolution (1 km) mapping of the impact of various drivers on heat-related deaths in cities, addressing a gap in previous studies that primarily focused on city-level or coarse spatial resolutions (Table 1). Our high-resolution mapping facilitates a more accurate assessment of the effectiveness of landscape-level strategies aimed at reducing heat-related deaths along the urban-rural gradient, which can also be recognized as the high-low population density gradient in China. Our findings indicate that landscape-level strategies are likely to be more effective in mitigating heat-related deaths within densely populated urban settlements of high-income megacities. In summary, our study highlights the critical role of high-resolution spatial analysis and landscape-level strategies in reducing heat-related mortality, offering implications for future research, policy development, and urban planning to enhance public health outcomes in the face of rising temperatures.

Acknowledgments

This work was supported by the National Natural Science Foundation of China (Grant No. 42130107 and 42201309), the Humanity and Social Science Youth Foundation of Ministry of Education of China (Grant No. 22YJCZH113), and the Shanghai Soft Science Program (Grant No. 23692113500). The funders played no role in the study design or data collection, management, analysis or interpretation, review or approval; or the decision to submit the manuscript for publication.

Xue Liu contributed to the study design, analysis performance, and draft writing; Y.Z. contributed to the study design and draft writing; M.H., Y.Z., Z.X., Xiaojuan Liu, Y.G., R.L., and H.Z. contributed to analysis performance; Xia Li contributed to the study design and draft writing; Xiaoping Liu contributed to the draft writing; and Y.Y. contributed to the study design, analysis performance, and draft writing.

References

1. Burke M, González F, Baylis P, Heft-Neal S, Baysan C, Basu S, et al. 2018. Higher temperatures increase suicide rates in the United States and Mexico. Nat Clim Chang 8(8):723–729, https://doi.org/10.1038/s41558-018-0222-x.
2. Ebi KL, Capon A, Berry P, Broderick C, de Dear R, Havenith G, et al. 2021. Hot weather and heat extremes: health risks. Lancet 398(10301):698–708, PMID: 34419205, https://doi.org/10.1016/S0140-6736(21)01208-3.
3. Raymond C, Matthews T, Horton RM. 2020. The emergence of heat and humidity too severe for human tolerance. Sci Adv 6(19):eaaw1838, PMID: 32494693, https://doi.org/10.1126/sciadv.aaw1838.
4. Barriopedro D, Fischer EM, Luterbacher J, Trigo RM, García-Herrera R. 2011. The hot summer of 2010: redrawing the temperature record map of Europe. Science 332(6026):220–224, PMID: 21415316, https://doi.org/10.1126/science.1201224.
5. Jay O, Capon A, Berry P, Broderick C, de Dear R, Havenith G, et al. 2021. Reducing the health effects of hot weather and heat extremes: from personal cooling strategies to green cities. Lancet 398(10301):709–724, PMID: 34419206, https://doi.org/10.1016/S0140-6736(21)01209-5.
6. Iungman T, Cirach M, Marando F, Pereira Barboza E, Khomenko S, Masselot P, et al. 2023. Cooling cities through urban green infrastructure: a health impact assessment of European cities. Lancet 401(10376):577–589, PMID: 36736334, https://doi.org/10.1016/S0140-6736(22)02585-5.
7. Mazdiyasni O, AghaKouchak A, Davis SJ, Madadgar S, Mehran A, Ragno E, et al. 2017. Increasing probability of mortality during Indian heat waves. Sci Adv 3(6): e1700066, PMID: 28630921, https://doi.org/10.1126/sciadv.1700066.
8. Raftery AE, Zimmer A, Frierson DMW, Startz R, Liu P. 2017. Less than 2°C warming by 2100 unlikely. Nat Clim Chang 7:637–641, PMID: 30079118, https://doi.org/10.1038/nclimate3352.
9. Romanello M, McGushin A, Di Napoli C, Drummond P, Hughes N, Jamart L, et al. 2021. The 2021 report of the *Lancet* Countdown on health and climate change: code red for a healthy future. Lancet 398(10311):1619–1662, PMID: 34687662, https://doi.org/10.1016/S0140-6736(21)01787-6.
10. Yang J, Zhou M, Ren Z, Li M, Wang B, Liu DL, et al. 2021. Projecting heat-related excess mortality under climate change scenarios in China. Nat Commun 12(1):1039, PMID: 33589602, https://doi.org/10.1038/s41467-021-21305-1.
11. Wang Y, Wang A, Zhai J, Tao H, Jiang T, Su B, et al. 2019. Tens of thousands additional deaths annually in cities of China between 1.5 °C and 2.0 °C warming. Nat Commun 10(1):3376, PMID: 31388009, https://doi.org/10.1038/s41467-019-11283-w.
12. Rai M, Breitner S, Wolf K, Peters A, Schneider A, Chen K. 2022. Future temperature-related mortality considering physiological and socioeconomic adaptation: a modelling framework. Lancet Planet Health 6(10):e784–e792, PMID: 36208641, https://doi.org/10.1016/S2542-5196(22)00195-4.
13. Chen H, Zhao L, Cheng L, Zhang Y, Wang H, Gu K, et al. 2022. Projections of heatwave-attributable mortality under climate change and future population scenarios in China. Lancet Reg Health West Pac 28:100582, PMID: 36105236, https://doi.org/10.1016/j.lanwpc.2022.100582.
14. Hathway EA, Sharples S. 2012. The interaction of rivers and urban form in mitigating the urban heat island effect: a UK case study. Build Environ 58:14–22, https://doi.org/10.1016/j.buildenv.2012.06.013.
15. Heaviside C, Vardoulakis S, Cai XM. 2016. Attribution of mortality to the urban heat island during heatwaves in the West Midlands, UK. Environ Health 15 Suppl 1(suppl 1):27, PMID: 26961286, https://doi.org/10.1186/s12940-016-0100-9.
16. Li H, Meier F, Lee X, Chakraborty T, Liu J, Schaap M, et al. 2018. Interaction between urban heat island and urban pollution island during summer in Berlin. Sci Total Environ 636:818–828, PMID: 29727848, https://doi.org/10.1016/j.scitotenv.2018.04.254.
17. Liu X, Ming Y, Liu Y, Yue W, Han G. 2022. Influences of landform and urban form factors on urban heat island: comparative case study between Chengdu and Chongqing. Sci Total Environ 820:153395, PMID: 35081410, https://doi.org/10.1016/j.scitotenv.2022.153395.
18. Huang K, Li X, Liu X, Seto KC. 2019. Projecting global urban land expansion and heat island intensification through 2050. Environ Res Lett 14(11):114037, https://doi.org/10.1088/1748-9326/ab4b71.
19. Manoli G, Fatichi S, Schläpfer M, Yu K, Crowther TW, Meili N, et al. 2019. Magnitude of urban heat islands largely explained by climate and population. Nature 573(7772):55–60, PMID: 31485056, https://doi.org/10.1038/s41586-019-1512-9.
20. Hsu A, Sheriff G, Chakraborty T, Manya D. 2021. Disproportionate exposure to urban heat island intensity across major US cities. Nat Commun 12(1):2721, PMID: 34035248, https://doi.org/10.1038/s41467-021-22799-5.
21. Zhu D, Zhou Q, Liu M, Bi J. 2021. Non-optimum temperature-related mortality burden in China: addressing the dual influences of climate change and urban heat islands. Sci Total Environ 782:146760, PMID: 33836376, https://doi.org/10.1016/j.scitotenv.2021.146760.
22. Hajat S, Proestos Y, Araya-Lopez JL, Economou T, Lelieveld J. 2023. Current and future trends in heat-related mortality in the MENA region: a health impact assessment with bias-adjusted statistically downscaled CMIP6 (SSP-based) data and Bayesian inference. Lancet Planet Health 7(4):e282–e290, PMID: 37019569, https://doi.org/10.1016/S2542-5196(23)00045-1.
23. Jenkins K, Kennedy-Asser A, Andrews O, Lo YTE. 2022. Updated projections of UK heat-related mortality using policy-relevant global warming levels and socioeconomic scenarios. Environ Res Lett 17(11):114036, https://doi.org/10.1088/1748-9326/ac9cf3.
24. Rodrigues M, Santana P, Rocha A. 2020. Modelling climate change impacts on attributable-related deaths and demographic changes in the largest metropolitan area in Portugal: a time-series analysis. Environ Res 190:109998, PMID: 32771365, https://doi.org/10.1016/j.envres.2020.109998.
25. Marando F, Heris MP, Zulian G, Udías A, Mentaschi L, Chrysoulakis N, et al. 2022. Urban heat island mitigation by green infrastructure in European functional urban areas. Sustain Cities Soc 77:103564, https://doi.org/10.1016/j.scs.2021.103564.
26. Onishi A, Cao X, Ito T, Shi F, Imura H. 2010. Evaluating the potential for urban heat-island mitigation by greening parking lots. Urban Forest Urban Green 9(4):323–332, https://doi.org/10.1016/j.ufug.2010.06.002.
27. Santamouris M, Ding L, Fiorito F, Oldfield P, Osmond P, Paolini R, et al. 2017. Passive and active cooling for the outdoor built environment–analysis and assessment of the cooling potential of mitigation technologies using performance data from 220 large scale projects. Solar Energy 154:14–33, https://doi.org/10.1016/j.solener.2016.12.006.
28. Santamouris M, Fiorito F. 2021. On the impact of modified urban albedo on ambient temperature and heat related mortality. Solar Energy 216:493–507, https://doi.org/10.1016/j.solener.2021.01.031.
29. Santamouris M. 2014. Cooling the cities–a review of reflective and green roof mitigation technologies to fight heat island and improve comfort in urban environments. Solar Energy 103:682–703, https://doi.org/10.1016/j.solener.2012.07.003.
30. Wang Y, Berardi U, Akbari H. 2016. Comparing the effects of urban heat island mitigation strategies for Toronto, Canada. Energy Build 114:2–19, https://doi.org/10.1016/j.enbuild.2015.06.046.
31. Aboubakri O, Khanjani N, Jahani Y, Bakhtiari B, Mesgari E. 2020. Projection of mortality attributed to heat and cold; the impact of climate change in a dry region of Iran, Kerman. Sci Total Environ 728:138700, PMID: 32361360, https://doi.org/10.1016/j.scitotenv.2020.138700.
32. Hondula DM, Georgescu M, Balling RC. 2014. Challenges associated with projecting urbanization-induced heat-related mortality. Sci Total Environ 490:538–544, PMID: 24880543, https://doi.org/10.1016/j.scitotenv.2014.04.130.
33. O'Neill BC, Tebaldi C, van Vuuren DP, Eyring V, Friedlingstein P, Hurtt G, et al. 2016. The scenario model intercomparison project (ScenarioMIP) for CMIP6. Geosci Model Dev 9(9):3461–3482, https://doi.org/10.5194/gmd-9-3461-2016.
34. Alahmad B, Vicedo-Cabrera AM, Chen K, Garshick E, Bernstein AS, Schwartz J, et al. 2022. Climate change and health in Kuwait: temperature and mortality projections under different climatic scenarios. Environ Res Lett 17(7):074001, https://doi.org/10.1088/1748-9326/ac7601.
35. de Schrijver E, Sivaraj S, Raible CC, Franco OH, Chen K, Vicedo-Cabrera AM. 2023. Nationwide projections of heat- and cold-related mortality impacts under various climate change and population development scenarios in Switzerland. Environ Res Lett 18(9):094010, PMID: 38854588, https://doi.org/10.1088/1748-9326/ace7e1.
36. Khatana SAM, Eberly LA, Nathan AS, Groeneveld PW. 2023. Projected change in the burden of excess cardiovascular deaths associated with extreme heat by midcentury (2036–2065) in the contiguous United States. Circulation 148(20):1559–1569, PMID: 37901952, https://doi.org/10.1161/CIRCULATIONAHA.123.066017.
37. Liu J, Dong H, Li M, Wu Y, Zhang C, Chen J, et al. 2023. Projecting the excess mortality due to heatwave and its characteristics under climate change, population and adaptation scenarios. Int J Hyg Environ Health 250:114157, PMID: 36989996, https://doi.org/10.1016/j.ijheh.2023.114157.
38. Thrasher B, Maurer EP, McKellar C, Duffy PB. 2012. Technical note: bias correcting climate model simulated daily temperature extremes with quantile mapping. Hydrol Earth Syst Sci 16(9):3309–3314, https://doi.org/10.5194/hess-16-3309-2012.
39. Pesaresi M, Ehrlich D, Ferri S, Florczyk A, Carneiro Freire S, Halkia S, et al. 2016. Operating procedure for the production of the Global Human Settlement Layer from Landsat data of the epochs 1975, 1990, 2000, and 2014. Luxembourg: Publications Office of the European Union, 1–62.
40. Menne MJ, Durre I, Vose RS, Gleason BE, Houston TG. 2012. An overview of the global historical climatology network-daily database. J Atmos Ocean Technol 29(7):897–910, https://doi.org/10.1175/JTECH-D-11-00103.1.
41. Gong P, Li X, Wang J, Bai Y, Chen B, Hu T, et al. 2020. Annual maps of global artificial impervious area (GAIA) between 1985 and 2018. Remote Sens Environ 236:111510, https://doi.org/10.1016/j.rse.2019.111510.
42. Chen G, Li X, Liu X, Chen Y, Liang X, Leng J, et al. 2020. Global projections of future urban land expansion under shared socioeconomic pathways. Nat Commun 11(1):537, PMID: 31988288, https://doi.org/10.1038/s41467-020-14386-x.

43. Li M, Zhou B-B, Gao M, Chen Y, Hao M, Hu G, et al. 2022. Spatiotemporal dynamics of global population and heat exposure (2020–2100): based on improved SSP-consistent population projections. Environ Res Lett 17(9):094007, https://doi.org/10.1088/1748-9326/ac8755.
44. Wang T, Sun F. 2022. Global gridded GDP data set consistent with the shared socioeconomic pathways. Sci Data 9(1):221, PMID: 35589734, https://doi.org/10.1038/s41597-022-01300-x.
45. Gunawardena KR, Wells MJ, Kershaw T. 2017. Utilising green and bluespace to mitigate urban heat island intensity. Sci Total Environ 584-585:1040–1055, PMID: 28161043, https://doi.org/10.1016/j.scitotenv.2017.01.158.
46. Ballester J, Quijal-Zamorano M, Méndez Turrubiates RF, Pegenaute F, Herrmann FR, Robine JM, et al. 2023. Heat-related mortality in Europe during the summer of 2022. Nat Med 29(7):1857–1866, PMID: 37429922, https://doi.org/10.1038/s41591-023-02419-z.
47. Hempel S, Frieler K, Warszawski L, Schewe J, Piontek F. 2013. A trend-preserving bias correction – the ISI-MIP approach. Earth Syst Dynam 4(2):219–236, https://doi.org/10.5194/esd-4-219-2013.
48. Lay CR, Sarofim MC, Vodonos Zilberg A, Mills DM, Jones RW, Schwartz J, et al. 2021. City-level vulnerability to temperature-related mortality in the USA and future projections: a geographically clustered meta-regression. Lancet Planet Health 5(6):e338–e346, PMID: 34022145, https://doi.org/10.1016/S2542-5196(21)00058-9.
49. Petkova EP, Vink JK, Horton RM, Gasparrini A, Bader DA, Francis JD, et al. 2017. Towards more comprehensive projections of urban heat-related mortality: estimates for New York City under multiple population, adaptation, and climate scenarios. Environ Health Perspect 125(1):47–55, PMID: 27337737, https://doi.org/10.1289/EHP166.
50. Zhang X, Friedl MA, Schaaf CB, Strahler AH, Schneider A. 2004. The footprint of urban climates on vegetation phenology. Geophys Res Lett 31(12):L12209, https://doi.org/10.1029/2004GL020137.
51. Li X, Zhou Y, Asrar GR, Imhoff M, Li X. 2017. The surface urban heat island response to urban expansion: a panel analysis for the conterminous United States. Sci Total Environ 605-606:426–435, PMID: 28672231, https://doi.org/10.1016/j.scitotenv.2017.06.229.
52. Imhoff ML, Zhang P, Wolfe RE, Bounoua L. 2010. Remote sensing of the urban heat island effect across biomes in the continental USA. Remote Sens Environ 114(3):504–513, https://doi.org/10.1016/j.rse.2009.10.008.
53. Li Y, Schubert S, Kropp JP, Rybski D. 2020. On the influence of density and morphology on the urban heat island intensity. Nat Commun 11(1):2647, PMID: 32461547, https://doi.org/10.1038/s41467-020-16461-9.
54. Zhou B, Rybski D, Kropp JP. 2013. On the statistics of urban heat island intensity. Geophys Res Lett 40(20):5486–5491, https://doi.org/10.1002/2013GL057320.
55. Lin X, Zhang W, Huang Y, Sun W, Han P, Yu L, et al. 2016. Empirical estimation of near-surface air temperature in China from MODIS LST data by considering physiographic features. Remote Sens 8(8):629, https://doi.org/10.3390/rs8080629.
56. Li H, Zhou Y, Li X, Meng L, Wang X, Wu S, et al. 2018. A new method to quantify surface urban heat island intensity. Sci Total Environ 624:262–272, PMID: 29253774, https://doi.org/10.1016/j.scitotenv.2017.11.360.
57. Li H, Zhou Y, Jia G, Zhao K, Dong J. 2022. Quantifying the response of surface urban heat island to urbanization using the annual temperature cycle model. Geosci Front 13(1):101141, https://doi.org/10.1016/j.gsf.2021.101141.
58. Li X, Gong P, Zhou Y, Wang J, Bai Y, Chen B, et al. 2020. Mapping global urban boundaries from the global artificial impervious area (GAIA) data. Environ Res Lett 15(9):094044, https://doi.org/10.1088/1748-9326/ab9be3.
59. Peng J, Hu Y, Liu Y, Ma J, Zhao S. 2018. A new approach for urban-rural fringe identification: integrating impervious surface area and spatial continuous wavelet transform. Landsc Urban Plan 175:72–79, https://doi.org/10.1016/j.landurbplan.2018.03.008.
60. Qiao K, Zhu W, Hu D, Hao M, Chen S, Cao S. 2018. Examining the distribution and dynamics of impervious surface in different function zones in Beijing. J Geogr Sci 28(5):669–684, https://doi.org/10.1007/s11442-018-1498-5.
61. Zhou Y, Smith SJ, Zhao K, Imhoff M, Thomson A, Bond-Lamberty B, et al. 2015. A global map of urban extent from nightlights. Environ Res Lett 10(5):054011, https://doi.org/10.1088/1748-9326/10/5/054011.
62. Chen R, Yin P, Wang L, Liu C, Niu Y, Wang W, et al. 2018. Association between ambient temperature and mortality risk and burden: time series study in 272 main Chinese cities. BMJ 363:k4306, PMID: 30381293, https://doi.org/10.1136/bmj.k4306.
63. Huang Z, Lin H, Liu Y, Zhou M, Liu T, Xiao J, et al. 2015. Individual-level and community-level effect modifiers of the temperature–mortality relationship in 66 Chinese communities. BMJ Open 5(9):e009172, PMID: 26369803, https://doi.org/10.1136/bmjopen-2015-009172.
64. Ma W, Wang L, Lin H, Liu T, Zhang Y, Rutherford S, et al. 2015. The temperature–mortality relationship in China: an analysis from 66 Chinese communities. Environ Res 137:72–77, PMID: 25490245, https://doi.org/10.1016/j.envres.2014.11.016.
65. Wang C, Zhang Z, Zhou M, Wang P, Yin P, Ye W, et al. 2018. Different response of human mortality to extreme temperatures (MoET) between rural and urban areas: a multi-scale study across China. Health Place 50:119–129, PMID: 29432981, https://doi.org/10.1016/j.healthplace.2018.01.011.
66. Gasparrini A, Guo Y, Hashizume M, Lavigne E, Zanobetti A, Schwartz J, et al. 2015. Mortality risk attributable to high and low ambient temperature: a multicountry observational study. Lancet 386(9991):369–375, PMID: 26003380, https://doi.org/10.1016/S0140-6736(14)62114-0.
67. Liu J, Liu T, Burkart KG, Wang H, He G, Hu J, et al. 2022. Mortality burden attributable to high and low ambient temperatures in China and its provinces: results from the Global Burden of Disease Study 2019. Lancet Reg Health West Pac 24:100493, PMID: 35756888, https://doi.org/10.1016/j.lanwpc.2022.100493.
68. Zhang L, Zhang Z, Wang C, Zhou M, Yin P. 2017. Different mortality effects of extreme temperature stress in three large city clusters of northern and southern China. Int J Disaster Risk Sci 8(4):445–456, https://doi.org/10.1007/s13753-017-0149-2.
69. Yin Q, Wang J, Ren Z, Li J, Guo Y. 2019. Mapping the increased minimum mortality temperatures in the context of global climate change. Nat Commun 10(1):4640, PMID: 31604931, https://doi.org/10.1038/s41467-019-12663-y.
70. Sinha P, Coville RC, Hirabayashi S, Lim B, Endreny TA, Nowak DJ. 2021. Modeling lives saved from extreme heat by urban tree cover. Ecol Modell 449:109553, https://doi.org/10.1016/j.ecolmodel.2021.109553.
71. Pace R, Chiocchini F, Sarti M, Endreny TA, Calfapietra C, Ciolfi M. 2023. Integrating Copernicus land cover data into the i-Tree Cool Air model to evaluate and map urban heat mitigation by tree cover. Eur J Remote Sens 56(1), https://doi.org/10.1080/22797254.2022.2125833.
72. Yao Y, Tian H, Shi H, Pan S, Xu R, Pan N, et al. 2020. Increased global nitrous oxide emissions from streams and rivers in the Anthropocene. Nat Clim Chang 10(2):138–142, https://doi.org/10.1038/s41558-019-0665-8.
73. Chen K, Horton RM, Bader DA, Lesk C, Jiang L, Jones B, et al. 2017. Impact of climate change on heat-related mortality in Jiangsu Province, China. Environ Pollut 224:317–325, PMID: 28237309, https://doi.org/10.1016/j.envpol.2017.02.011.
74. Masselot P, Mistry M, Vanoli J, Schneider R, Iungman T, Garcia-Leon D, et al. EXHAUSTION project. 2023. Excess mortality attributed to heat and cold: a health impact assessment study in 854 cities in Europe. Lancet Planet Health 7(4):e271–e281, PMID: 36934727, https://doi.org/10.1016/S2542-5196(23)00023-2.
75. Ecob R, Smith GD. 1999. Income and health: what is the nature of the relationship? Soc Sci Med 48(5):693–705, PMID: 10080369, https://doi.org/10.1016/s0277-9536(98)00385-2.
76. Shibuya K, Hashimoto H, Yano E. 2002. Individual income, income distribution, and self rated health in Japan: cross sectional analysis of nationally representative sample. BMJ 324(7328):16–19, PMID: 11777798, https://doi.org/10.1136/bmj.324.7328.16.
77. Kondo MC, Mueller N, Locke DH, Roman LA, Rojas-Rueda D, Schinasi LH, et al. 2020. Health impact assessment of Philadelphia's 2025 tree canopy cover goals. Lancet Planet Health 4(4):e149–e157, PMID: 32353295, https://doi.org/10.1016/S2542-5196(20)30058-9.
78. Ng E, Chen L, Wang Y, Yuan C. 2012. A study on the cooling effects of greening in a high-density city: an experience from Hong Kong. Build Environ 47:256–271, https://doi.org/10.1016/j.buildenv.2011.07.014.
79. Aflaki A, Mirnezhad M, Ghaffarianhoseini A, Ghaffarianhoseini A, Omrany H, Wang Z-H, et al. 2017. Urban heat island mitigation strategies: a state-of-the-art review on Kuala Lumpur, Singapore and Hong Kong. Cities 62:131–145, https://doi.org/10.1016/j.cities.2016.09.003.
80. Cai Y, Li C, Ye L, Xiao L, Gao X, Mo L, et al. 2022. Effect of the roadside tree canopy structure and the surrounding on the daytime urban air temperature in summer. Agric For Meteorol 316:108850, https://doi.org/10.1016/j.agrformet.2022.108850.
81. Irmak MA, Yilmaz S, Mutlu E, Yilmaz H. 2018. Assessment of the effects of different tree species on urban microclimate. Environ Sci Pollut Res Int 25(16):15802–15822, PMID: 29582327, https://doi.org/10.1007/s11356-018-1697-8.
82. Rahman MA, Arndt S, Bravo F, Cheung PK, van Doorn N, Franceschi E, et al. 2024. More than a canopy cover metric: influence of canopy quality, water-use strategies and site climate on urban forest cooling potential. Landsc Urban Plan 248:105089, https://doi.org/10.1016/j.landurbplan.2024.105089.
83. Heaviside C, Macintyre H, Vardoulakis S. 2017. The urban heat island: implications for health in a changing environment. Curr Environ Health Rep 4(3):296–305, PMID: 28695487, https://doi.org/10.1007/s40572-017-0150-3.
84. Ramírez-Aguilar EA, Lucas Souza LC. 2019. Urban form and population density: influences on urban heat island intensities in Bogotá, Colombia. Urban Clim 29:100497, https://doi.org/10.1016/j.uclim.2019.100497.
85. Grant A, Millward AA, Edge S, Roman LA, Teelucksingh C. 2022. Where is environmental justice? A review of US urban forest management plans. Urban For Urban Green 77:127737, https://doi.org/10.1016/j.ufug.2022.127737.
86. Locke DH, Hall B, Grove JM, Pickett STA, Ogden LA, Aoki C, et al. 2021. Residential housing segregation and urban tree canopy in 37 US cities. NPJ Urban Sustain 1(1):15, https://doi.org/10.1038/s42949-021-00022-0.
87. Kephart JL, Sánchez BN, Moore J, Schinasi LH, Bakhtsiyarava M, Ju Y, et al. 2022. City-level impact of extreme temperatures and mortality in Latin America. Nat Med 28(8):1700–1705, PMID: 35760859, https://doi.org/10.1038/s41591-022-01872-6.